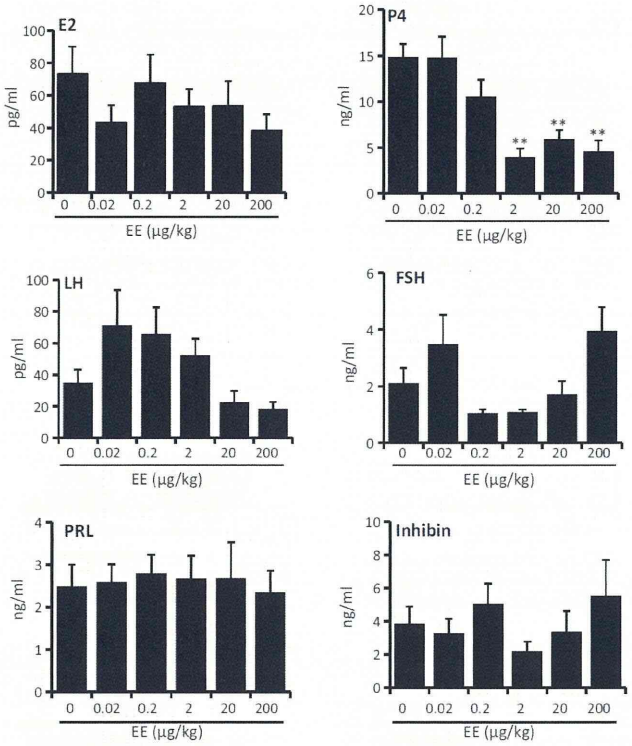

Fig. 4. Serum level of sex-related hormones at 10 months of age. Data are the mean ± SEM. $n = 22$ per each group. In the 0.02 μg/kg group, 2 animals were excluded due to tumors at weeks 36 and 42. **: Significantly different from the 0 μg/kg group at $p < 0.01$.

there are no studies covering the neonatal period to middle age.

To examine the long-term effects of neonatal exposure to EE, we performed histopathologic examinations of female reproductive organs at 10 months of age. A decrease or decreasing tendency of ovarian weight existed from the 0.2 μg/kg group, and histopathologic examinations revealed cystic atretic follicles and loss of corpus lutea in the same groups, which suggests anovulation. Such findings were also noted in the animals showing persistent estrous in the control and 0.02 μg/kg groups. Therefore, the morphologic changes induced by delayed adverse effects in the ovary were regarded as changes related to aging, rather than abnormalities specific to EE-treatment. In contrast, there was no obvious variation in the remaining primary and antral follicles and serum hormone levels secreted by follicles, such as E2 and inhibin, suggesting that anovulation is not caused by dysfunction of the ovary and depletion of reserve follicles.

Although no statistical differences were noted in the incidence and multiplicity of uterine atypical hyperplasia and adenocarcinoma, there was a tendency toward increased severity of lesions at ≧2 μg/kg. Moreover, the incidence of cystic endometrial hyperplasia was significantly elevated at 2 and 20 μg/kg. In these groups, the serum P4 level was significantly lowered due to a loss of corpus lutea by persistent anovulation. Because the serum E2 level was unchanged, the estrogen:progesterone (E:P) ratio was elevated in these groups after the onset of abnormal estrous cyclicity. A prolonged increase in the E:P ratio is regarded as an important factor for the development of endometrial adenocarcinoma in rodents, as well as humans [12,18–20]. Therefore, an increasing tendency toward severity of uterine proliferative lesions in the higher dose groups might be caused by an elevated E:P ratio. Similarly, previous studies reported that the early onset of persistent estrus and an increase in uterine adenocarcinoma were observed in Donryu rats that received a single injection of DES or high-dose *p-t*-octylphenol, an estrogenic chemical, during the neonatal period [2,21]. In addition, a significant increase in squamous metaplasia was apparent from 0.2 μg/kg, the dose associated with delayed adverse effects in estrous cyclicity. Prolonged estrogen exposure has been associated with squamous metaplasia in rats for many years; however, the precise underlying mechanism is not known [22]. Therefore, it is thought that the findings observed in the current study reflect hormonal imbalance (a reduction in P4 relative to E2) due to the early onset of anovulation.

At the highest dose of EE, disappearance of the lumen occurred in one case. Similar morphologic abnormalities were reported in rats that had neonatal exposure to high doses of DES [2]. Adenomyosis is commonly observed in aging GALAS rats, and the incidence is 12–40% in the 1- or 2-year toxicity studies in our laboratory (data not shown). In the present study, the incidences of adenomyosis in the control and low- or middle-dose groups were similar to

our background data, but the incidence in high-dose groups was decreased. It is known that early postnatal exposure to estrogenic compounds can suppress uterine gland genesis and expression of estrogen receptors, and can alter the uterine response to estrogen [23–25]. Therefore, development of uterine glands might be affected by neonatal exposure to EE, especially at high doses, and lead to a decrease in adenomyosis. Although the absolute and relative weights of the uterus were significantly elevated at 0.02 μg/kg, the toxicologic significance is not known because there were no histologic findings related to the increase in uterine weight and uterine weights in the higher dose groups were not changed.

Neonatal exposure to EE did not affect the proliferative lesions in the anterior pituitary and serum level of pituitary hormones, including PRL. In addition, there were no intergroup differences in the incidence and severity of milk secretion in the mammary glands. In the 20 μg/kg group, the incidence of atypical hyperplasia was increased, and neoplastic lesions, such as adenomas and fibroadenomas, were only found from 20 μg/kg. Neonatal exposure to DES in rats has been reported to affect mammary carcinogenesis, although the types of tumors induced varied by dose and timing [26]; the cause remained undetermined, but the increase in atypical hyperplasia at 20 μg/kg, the inducible level of delayed effects, might be related to EE-treatment. In contrast, an increase in acini exhibiting oxyphilic and hypertrophic changes (virilization) was observed from 0.2 μg/kg in a dose-dependent manner. It has been reported that virilization of mammary acini appeared in female rats that received neonatal administration of DES [26,27]. In these studies, oxyphilic changes were noted in rats administered DES from PND 0-14 and PND 0-5, whereas rats administered DES from PND 6-14 did not exhibit such a change. Therefore, the critical period of endocrine disruptors affecting mammary morphology was thought to be from 0 to 5 days after birth. In a recent report similar to our study, changes in the mammary glands such as milk accumulations and hyperplasia were found in adult rats received single neonatal exposure to EE [28]. Accordingly, although precise mechanisms remain unknown, it was thought that neonatal exposure to EE is likely to have some effects on development of mammary glands directly and resulted in oxyphilic changes in the current study.

The critical mechanism underlying the early onset of abnormal estrous cycles is unknown; however, dysfunction of the ovulation center in the hypothalamus is presumed to be a possible mechanism regulating anovulation, because there were no intergroup differences in the remaining follicles in the ovary and the serum levels of pituitary hormones, such as FSH, LH, and PRL, at 10 months of age. Kisspeptin, which is expressed in specific neurons in the anteroventral periventricular nucleus and arcuate nucleus of the hypothalamus, is widely recognized to play a critical role in female reproductive function, including regulation of ovulation and estrous cyclicity [29,30]. It has been reported that neonatal injection of estradiol benzoate to male and female rats results in a dose-dependent decrease in hypothalamic kiss-1 mRNA levels in the prepubertal stage, which is linked to lowering of serum LH concentrations [31]. Therefore, neurons expressing kisspeptin might be a target of neonatal exposure to EE. Research to elucidate the relationship between the expression of the kiss-1 gene and delayed adverse effects is now in progress in our laboratory.

5. Conclusion

In summary, our results clearly demonstrated that neonatal exposure to EE at doses of 0.2–200 μg/kg, which exert estrogenic activity *in vivo*, induces early onset of anovulation in a dose-dependent fashion after sexual maturation. Estrous cyclicity is regarded as a very useful indicator of delayed adverse effects on the female reproductive tract. Dysfunction of the ovulation center in the hypothalamus is presumed to be a possible mechanism underlying the early onset of anovulation based on the lack of abnormalities in the remaining follicles and pituitary hormones, although the precise mechanism has not been delineated. As a long-term effect derived from the early onset of anovulation, it is suggested that prolonged estrogen exposure might increase the risk for uterine carcinogenesis. In contrast, there was a possibility that neonatal exposure to EE could directly affect development of mammary glands.

Conflict of interest statement

The authors have no conflict of interest.

Acknowledgments

We thank Mss. Ayako Saikawa and Yoshimi Komatsu for technical assistance in conducting the animal study. This study was supported by Health and Labor Sciences Research Grants, Research on Risk of Chemical Substances, Ministry of Health, Labor and Welfare, Japan [H22-Toxicol-003].

References

[1] Gore AC, Walker DM, Zama AM, Armenti AE, Uzumcu M. Early life exposure to endocrine-disrupting chemicals causes lifelong molecular reprogramming of the hypothalamus and premature reproductive aging. Molecular Endocrinology 2011;25:2157–68.
[2] Yoshida M, Takahashi M, Inoue K, Hayashi S, Maekawa A, Nishikawa A. Delayed adverse effects of neonatal exposure to diethylstilbestrol and their dose dependency in female rats. Toxicologic Pathology 2011;39:823–34.
[3] Dickerson SM, Cunningham SL, Patisaul HB, Woller MJ, Gore AC. Endocrine disruption of brain sexual differentiation by developmental PCB exposure. Endocrinology 2011;152:581–94.
[4] Newbold RR, Bullock BC, McLachlan JA. Uterine adenocarcinoma in mice following developmental treatment with estrogens: a model for hormonal carcinogenesis. Cancer Research 1990;50:7677–81.
[5] Newbold RR. Developmental exposure to endocrine-disrupting chemicals programs for reproductive tract alterations and obesity later in life. American Journal of Clinical Nutrition 2011;94:1939S–42S.
[6] Herbst AL, Anderson D. Clear cell adenocarcinoma of the vagina and cervix secondary to intrauterine exposure to diethylstilbestrol. Seminars in Surgical Oncology 1990;6:343–6.
[7] Swan SH. Intrauterine exposure to diethylstilbestrol: long-term effects in humans. APMIS 2000;108:793–804.
[8] Düsterberg B, Kühne G, Täuber U. Half-lives in plasma and bioavailability of ethinylestradiol in laboratory animals. Arzneimittel-Forschung 1986;36:1187–90.
[9] Kanno J, Onyon L, Haseman J, Fenner-Crisp P, Ashby J, Owens W. Organisation for economic co-operation and development. The OECD program to validate the rat uterotrophic bioassay to screen compounds for in vivo estrogenic responses: phase 1. Environmental Health Perspectives 2001;109:785–94.
[10] DiGiovanni J. Modification of multistage skin carcinogenesis in mice. Progress in Experimental Tumor Research 1991;33:192–229.
[11] Imaida K, Fukushima S. Initiation-promotion model for assessment of carcinogenicity: medium-term liver bioassay in rats for rapid detection of carcinogenic agents. Journal of Toxicological Sciences 1996;21:483–7.
[12] Ando-Lu J, Takahashi M, Imai S, Ishihara R, Kitamura T, Iijima T, Takano S, Nishiyama K, Suzuki K, Maekawa A. High-yield induction of uterine endometrial adenocarcinomas in Donryu rats by a single intra-uterine administration of N-ethyl-N'-nitro-N-nitrosoguanidine via the vagina. Japanese Journal of Cancer Research 1994;85:789–93.
[13] Taya K, Mizokawa T, Matsui T, Sasamoto S. Induction of superovulation in prepubertal female rats by anterior pituitary transplants. Journal of Reproduction and Fertility 1983;69:265–70.
[14] Gibori G, Antczak E, Rothchild I. The role of estrogen in the regulation of luteal progesterone secretion in the rat after day 12 of pregnancy. Endocrinology 1977;100:1483–95.
[15] Korenman SG, Stevens RH, Carpenter LA, Robb M, Niswender GD, Sherman BM. Estradiol radioimmunoassay without chromatography: procedure, validation and normal values. Journal of Clinical Endocrinology and Metabolism 1974;38:718–20.
[16] Taya K, Watanabe G, Sasamoto S. Radioimmunoassay for progesterone, testosterone, and estradiol-17b using 125I-iodohistamine radioligands. Japan Journal of Animal Reproduction 1985;31:186–97.
[17] Hamada T, Watanabe G, Kokuho T, Taya K, Sasamoto S, Hasegawa Y, Miyamoto K, Igarashi M. Radioimmunoassay of inhibin in various mammals. Journal of Endocrinology 1989;122:697–704.

[18] Sekiya S, Iwasaki H, Takeda B, Takamizawa H. Endometrial carcinoma following chronic anovulation in a premenopausal woman with systemic lupus erythematosus. Acta Obstetricia et Gynecologica Scandinavica 1988;67:553–6.
[19] Niwa K, Tanaka T, Mori H, Yokoyama Y, Furui T, Mori H, Tamaya T. Rapid induction of endometrial carcinoma in ICR mice treated with N-methyl-N-nitrosourea and 17 beta-estradiol. Japanese Journal of Cancer Research 1991;82:1391–6.
[20] Modan B, Ron E, Lerner-Geva L, Blumstein T, Menczer J, Rabinovici J, Oelsner G, Freedman L, Mashiach S, Lunenfeld B. Cancer incidence in a cohort of infertile women. American Journal of Epidemiology 1998;147:1038–42.
[21] Yoshida M, Katsuda S, Tanimoto T, Asai S, Nakae D, Kurokawa Y, Taya K, Maekawa A. Induction of different types of uterine adenocarcinomas in Donryu rats due to neonatal exposure to high-dose p-t-octylphenol for different periods. Carcinogenesis 2002;23:1745–50.
[22] Mceuen CS. Metaplasia of uterine epithelium produced in rats by prolonged administration of oestrin. American Journal of Cancer 1936;27:91–4.
[23] Branham WS, Zehr DR, Chen JJ, Sheehan DM. Uterine abnormalities in rats exposed neonatally to diethylstilbestrol, ethynylestradiol, or clomiphene citrate. Toxicology 1988;51:201–12.
[24] Yoshida A, Newbold RR, Dixon D. Effects of neonatal diethylstilbestrol (DES) exposure on morphology and growth patterns of endometrial epithelial cells in CD-1 mice. Toxicologic Pathology 1999;27:325–33.
[25] Newbold RR, Jefferson WN, Padilla-Banks E, Haseman J. Developmental exposure to diethylstilbestrol (DES) alters uterine response to estrogens in prepubescent mice: low versus high dose effects. Reproductive Toxicology 2004;18:399–406.
[26] Kawaguchi H, Umekita Y, Souda M, Gejima K, Kawashima H, Yoshikawa T, Yoshida H. Effects of neonatally administered high-dose diethylstilbestrol on the induction of mammary tumors induced by 7,12-dimethylbenz[a]anthracene in female rats. Veterinary Pathology 2009;46:142–50.
[27] Yoshikawa T, Kawaguchi H, Umekita Y, Souda M, Gejima K, Kawashima H, Nagata R, Yoshida H. Effects of neonatally administered low-dose diethylstilbestrol on the induction of mammary carcinomas and dysplasias induced by 7,12-dimethylbenz [a] anthracene in female rats. In Vivo 2008;22:207–13.
[28] Shirota M, Kawashima J, Nakamura T, Ogawa Y, Kamiie J, Yasuno K, Shirota K, Yoshida M. Delayed effects of single neonatal subcutaneous exposure of low-dose 17α-ethynylestradiol on reproductive function in female rats. Journal of Toxicological Sciences 2012;37:681–90.
[29] Uenoyama Y, Tsukamura H, Maeda KI. Kisspeptin/metastin: a key molecule controlling two modes of gonadotrophin-releasing hormone/luteinising hormone release in female rats. Journal of Neuroendocrinology 2009;21:299–304.
[30] Roa J, Navarro VM, Tena-Sempere M. Kisspeptins in reproductive biology: consensus knowledge and recent developments. Biology of Reproduction 2011;85:650–60.
[31] Navarro VM, Sánchez-Garrido MA, Castellano JM, Roa J, García-Galiano D, Pineda R, Aguilar E, Pinilla L, Tena-Sempere M. Persistent impairment of hypothalamic KiSS-1 system after exposures to estrogenic compounds at critical periods of brain sex differentiation. Endocrinology 2009;150:2359–67.

Experimental and Toxicologic Pathology 65 (2013) 863–873

Contents lists available at SciVerse ScienceDirect

Experimental and Toxicologic Pathology

journal homepage: www.elsevier.de/etp

Thickened area of external granular layer and Ki-67 positive focus are early events of medulloblastoma in *Ptch1*$^{+/-}$ mice

Saori Matsuo[a,d], Miwa Takahashi[a], Kaoru Inoue[a], Kei Tamura[a], Kaoru Irie[a], Yukio Kodama[b], Akiyoshi Nishikawa[c], Midori Yoshida[a,*]

[a] Division of Pathology, National Institute of Health Sciences, 1-18-1 Kamiyoga, Setagaya-ku, Tokyo 158-8501, Japan
[b] Division of Toxicology, National Institute of Health Sciences, 1-18-1 Kamiyoga, Setagaya-ku, Tokyo 158-8501, Japan
[c] Biological Safety Research Center, National Institute of Health Sciences, 1-18-1 Kamiyoga, Setagaya-ku, Tokyo 158-8501, Japan
[d] Pathogenetic Veterinary Science, United Graduate School of Veterinary Sciences, Gifu University, 1-1 Yanagido, Gifu-shi, Gifu 501-1193, Japan

ARTICLE INFO

Article history:
Received 3 September 2012
Received in revised form
26 November 2012
Accepted 14 December 2012

Keywords:
Cerebellar development
Granule cell precursors
Medulloblastoma
Patched1
Preneoplastic lesion
Sonic hedgehog

ABSTRACT

Patched1 (Ptch1) encodes a receptor for Sonic hedgehog (Shh) and is major gene related to human medulloblastoma (MB) in the Shh subgroup. MB is thought to arise from residual granule cell precursors (GCPs) located in the external granular layer (EGL) of the developing cerebellum. As the detailed preneoplastic changes of MB remain obscure, we immunohistochemically clarified the derived cell, early events of MBs, and the cerebellar developmental processes of *Ptch1*$^{+/-}$ (Ptch1) mice, an animal model of human MB of the Shh subgroup. In Ptch1 mice, the earliest proliferative lesions were detected at PND10 as focal thickened areas of outer layer of the EGL. This area was composed of GCP-like cells with atypia and nuclei disarrangement. In the latter cerebellar developmental period, GCP-like cell foci were detected at high incidence in the outermost area of the cerebellum. Their localization and morphological similarities indicated that the foci were derived from GCPs in the EGL. There were two types of the foci. A Ki-67-positive focus was found in Ptch1 mice only. This type resembled the GCPs in the outer layer of EGL characterized by having proliferating activity and a lack of neuronal differentiation. Another type of focus, Ki-67-negative, was observed in both genotypes and exhibited many of the same features of mature internal granule cells, suggesting that the focus had no preneoplastic potential. Due to morphological, immunohistochemical characteristics, our results indicate that the focal thickened area of EGL and Ki-67-positive foci are preneoplastic lesions of MB.

1. Introduction

Medulloblastoma (MB) is the most common malignant tumor in children which shows tremendous biological and clinical heterogeneity (Dhall, 2009; Hatten and Roussel, 2011; Jones et al., 2012). MB in humans is classified into four subtypes with distinct clinical, biological, and genetic profiles (Aref et al., 2012; Ellison et al., 2011; Jones et al., 2012; Kool et al., 2012; Mohan et al., 2012; Northcott et al., 2011). Molecular analysis of Sonic hedgehog (Shh) tumors in humans revealed activation of the Shh signaling pathway due to the loss of *Patched1 (Ptch1)* and mutations in other components of the Shh pathway. Approximately as high as 30% of MBs have mutations in Shh pathway components (Bhatia et al., 2012; Crawford et al., 2007; Klesse and Bowers, 2010; Oliver et al., 2005; Roussel and Hatten, 2011; Wang et al., 2012). *Ptch1* encodes a receptor for Shh, Patched1 (Ptch1), and is one of the major genes related to MB formation in humans (Dhall, 2009; Raffel, 2004). A subset of MBs has been identified with allelic loss of chromosome 9q22, a region that contains *Ptch1* (Dhall, 2009; Raffel, 2004). Pathway activation is triggered by binding of Shh to Ptch1, which in the absence of Shh suppresses the activity of Smoothened (Smo). Shh binding to Ptch1 or mutational inactivation of Ptch1 relieves the inhibition of Smo culminating in the activation of one or more of the Gli1 transcription factors that regulate the expression of downstream targets (Huse and Holland, 2010; Roussel and Hatten, 2011). Inappropriate activation of the Shh pathway is accepted as a cause of familial cancer due to inherited mutation of the *Ptch1* gene, which has been identified as responsible for nevoid basal cell carcinoma syndrome (Dhall, 2009; Klesse and Bowers, 2010).

Heterozygous *Ptch1* knockout mice (Ptch1 mice) display many of the typical symptoms of nevoid basal cell carcinoma syndrome, also known as Gorlin syndrome, including skeletal abnormalities, neural tube closure defects, a generalized over-growth, and predisposition to tumor formation (Corcoran and Scott, 2001; Hahn et al., 1999; Raffel, 2004). In addition, the Ptch1 mouse strain displays a high yield (14% up to 30%) of MB that resembles human

* Corresponding author. Tel.: +81 3 3700 9821; fax: +81 3 3700 1425.
E-mail address: modoriy@nihs.go.jp (M. Yoshida).

0940-2993/$ - see front matter © 2012 Elsevier GmbH. All rights reserved.
http://dx.doi.org/10.1016/j.etp.2012.12.005

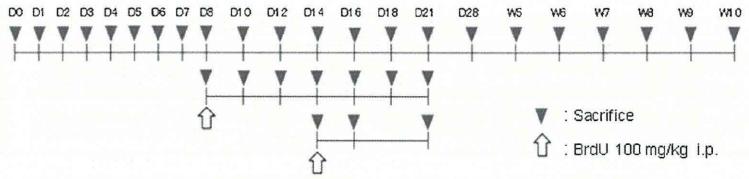

Fig. 1. Experimental design. Schedules for necropsy and the administration of BrdU are illustrated. Each time point represents at least 2 wild-type mice and 6 Ptch1 mice from over 2 dams. D, postnatal day; W, postnatal week.

MB of the Shh subgroup (Goodrich et al., 1997; Lau et al., 2012; Wetmore et al., 2000). In the mice, homozygous loss of *Ptch1* results in embryonic lethality at 9.5–10.5 days after fertilization (Goodrich et al., 1997). Thus, heterozygous *Ptch1* knockout mice have been used as a model for nevoid basal cell carcinoma/Gorlin syndrome including human MB, rhabdomyosarcoma, and basal cell carcinoma (Corcoran and Scott, 2001; Dyer, 2004; Hahn et al., 1999; Pazzaglia, 2006; Wu et al., 2011). Although Ptch1 mice are a valuable model for evaluation of drug efficacy and modulating effects of additional gene mutations, chemicals, or irradiation on brain tumor formation in childhood, the long latent period of 9 to over 12 months for assessment results in clinical signs of increased intracranial pressure (ataxia, decreased movement, paresis of hind limbs, enlarged occipital prominence, hunched back, and/or poor grooming) and death (Ayrault et al., 2009; Briggs et al., 2008; Ecke et al., 2008; Farioli-Vecchioli et al., 2007; Kimura et al., 2005; Pazzaglia et al., 2006, 2009; Pogoriler et al., 2006; Takahashi et al., 2012; Uziel et al., 2005; Wetmore et al., 2001). Therefore, detection of early indicators of MBs such as preneoplastic lesions in Ptch1 mice and evaluation with changes as an indicator of MB in short-term studies is needed.

To find early indicators of tumors in childhood, detailed investigation of normal developmental processes of target organs can be useful. Human MBs are thought to be derived from residual granule cell precursors (GCPs) located in the external granule cell or external granular (germinal) layer (EGL) of the cerebellum, although GCPs migrate inward to form the internal granule cell or internal granular layer (IGL) during normal cerebellar development (Behesti and Marino, 2009; Haldipur et al., 2012; Roussel and Hatten, 2011). The processes of cerebellar and MB development in Ptch1 mice are not well-defined.

This study was conducted to clarify the derived cell and early events of MBs, and cerebellar developmental processes in Ptch1 mice. We examined cerebella of Ptch1 mice and wild-type littermates sequentially during postnatal day (PND) 0 to 10 weeks of age.

2. Materials and methods

2.1. Animals

Ptch1 heterozygous knockout mice, generated by replacing exon 1 and 2 of the ptch1 gene with a LacZ/neomycin cassette (Goodrich et al., 1997), were obtained from The Jackson Laboratory (Bar Harbor, ME, USA) and maintained in our laboratory. They were housed in polycarbonate cages with wood chip bedding and maintained in an air-conditioned animal room (temperature 24 ± 1 °C, relative humidity 55 ± 5%, 12-h light–dark cycle) with basal diet (CRF-1, Oriental Yeast Co., Tokyo, Japan) and tap water available *ad libitum*. The experimental protocol using animals was reviewed and approved by the Animal Care and Use Committee of the National Institute of Health Sciences, Japan.

2.2. Necropsy

To examine following morphologic analysis necropsy was performed according to protocol (Fig. 1). Ptch1 and wild-type littermate mice were euthanized under deep anesthesia with isoflurane. 2–11 wild-type mice and 6–19 Ptch1 mice were analyzed at each time point from at least two litters.

2.3. Genotyping

Animals were genotyped by PCR amplification of genomic DNA extracted from the tail. The wild type allele was distinguished with primers 5′-CTG CGG CAA GTT TTT GGT TG-3′ and 5′-AGG GCT TCT CGT TGG CTA CAA G-3′, which yield a 200-bp PCR product. The mutant allele was detected using primers 5′-GCC CTG AAT GAA CTG CAG GAC G-3′ and 5′-CAC GGG TAG CCA ACG CTA TGT C-3′, which yield a 479-bp PCR product.

2.4. BrdU labeling

To examine migration of GCPs, a single intraperitoneal injection of 100 mg/kg body weight of 5-Bromo-2′-deoxyuridine (BrdU, CAS No. 59-14-3 Sigma–Aldrich, MO, USA) in saline (Otsuka Pharmaceutical Factory, Inc., Japan) was given to mice at PND8 and 14. Animals treated with BrdU at PND8 were euthanized as above 1.5 h after the injection and at PND10, 12, 14, 16, 18, and 21. Animals treated with BrdU at PND14 were euthanized 1.5 h after injection and at PND16 and 21 (Fig. 1).

Table 1
Primary antibodies used for immunohistochemistry.

Antigen	Clone	Concentration/dilution	Antigen retrieval	Visualization system	Source
BrdU	BU1/75(ICR1)	1 μg/mL	Autoclave	LSAB	AbD serotec
Ki-67	TEC-3	30 μg/mL	Autoclave	LSAB	Dako
NeuN	A60	3 μg/mL	Autoclave	Polymer	Millipore
$p27^{kip1}$	EP233(2)Y	1:2000	Autoclave	Polymer	Abcam
Nestin	Rat-401	3 μg/mL	Autoclave	Polymer	Millipore
CyclinD1	EPR2241(IHC)-32	1:300	Autoclave	Polymer	Millipore
GFAP	Polyclonal	1 μg/mL	Microwave	Polymer	Dako
Calbindin-D-28K	CB-955	3 μg/mL	Microwave	Polymer	Sigma–Aldrich

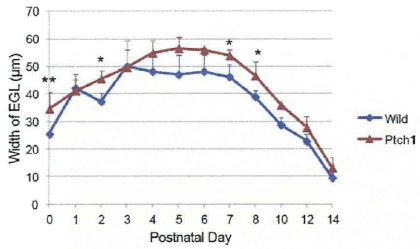

Fig. 2. Changes in the width of EGL in developing cerebellum of Ptch1 and wild-type mice from PND0 to PND14. *, **: Significantly different from wild-type mice at $P < 0.05$ and $P < 0.01$, respectively.

2.5. Tissue processing

After detailed necropsy, brains were removed and fixed in 10% neutral buffered formalin. Midsagittal sections of cerebella were routinely processed for paraffin embedding, sectioned and stained with hematoxylin and eosin. The prepared histopathological specimens were examined under light microscopy.

2.6. Morphometric assessment

Photomicrographs of midsagittal sections of the cerebellum were taken with a digital camera attached to microscope (DP71, Olympus Corp., Tokyo, Japan), and then measurement was performed using image analysis software (WinROOF, Version 5.7.1, Mitani Corp., Tokyo, Japan). The numbers of wild-type and Ptch1 mice measured at each time point were 3–6 obtained from 2 to 5 litters (mainly 3–5 litters) except for Ptch1 mice at PND10. At PND10, five mice were obtained from the same dam. The width of the EGL of each mouse was determined by five measurements selected at random from the entire cerebellum (PND0 to 2) or 4th/5th cerebellar lobules (PND3 to 14).

2.7. Immunohistochemistry

Antibodies used for immunohistochemistry included monoclonal rat anti-BrdU (AbD serotec, Oxford, UK), monoclonal rat anti-mouse Ki-67 (Dako Cytomation, Glostrup, Denmark) as proliferation marker, monoclonal mouse anti-NeuN (Millipore, MA, USA) as a mature granule cell marker, monoclonal rabbit anti-$p27^{kip1}$ (Abcam, Tokyo, Japan) as a postmitotic granule cell marker, monoclonal mouse anti-Nestin (Millipore) as a neuronal stem cell marker, monoclonal rabbit anti-CyclinD1 (Millipore) as a proliferating GCPs marker, polyclonal rabbit anti-GFAP (Dako Cytomation) as a Bergmann glia marker, and monoclonal mouse

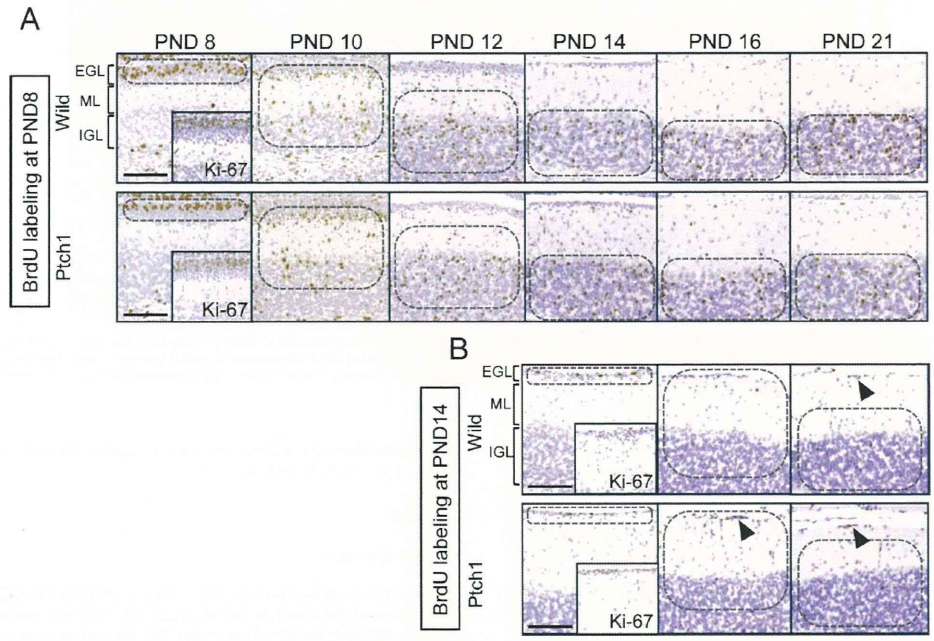

Fig. 3. Migration of GCPs of wild-type and Ptch1 mice from PND8 to PND21. (A) Sequential migration of GCPs labeled with BrdU at PND8 (1.5 h after injection) of wild-type (top row) and Ptch1 mice (bottom row). BrdU-positive cells were observed in Ki-67-positive, proliferating outer layers of the EGL 1.5 h later (PND8). At PND10 (2 days after injection), most of the BrdU-positive cells were localized in the inner layer of the EGL, molecular layer (ML), and IGL. The EGL almost disappeared at PND16 and most of the BrdU-positive cells finished migrating into the IGL by PND21. (B) Sequential migration of GCPs labeled with BrdU at PND14 of wild-type (top row) and Ptch1 mice (bottom row). BrdU-positive cells were observed in 1–3 layers of Ki-67-positive, proliferating cells of the EGL at PND14 (1.5 h after injection). From PND16 onwards when most of GCPs finished migrating from the EGL, small foci with GCP-like cells labeled with BrdU were detected in the outermost regions of cerebellar cortex (arrowhead). Circle indicates major location of BrdU-labeled GCPs. Scale bar: 100 μm.

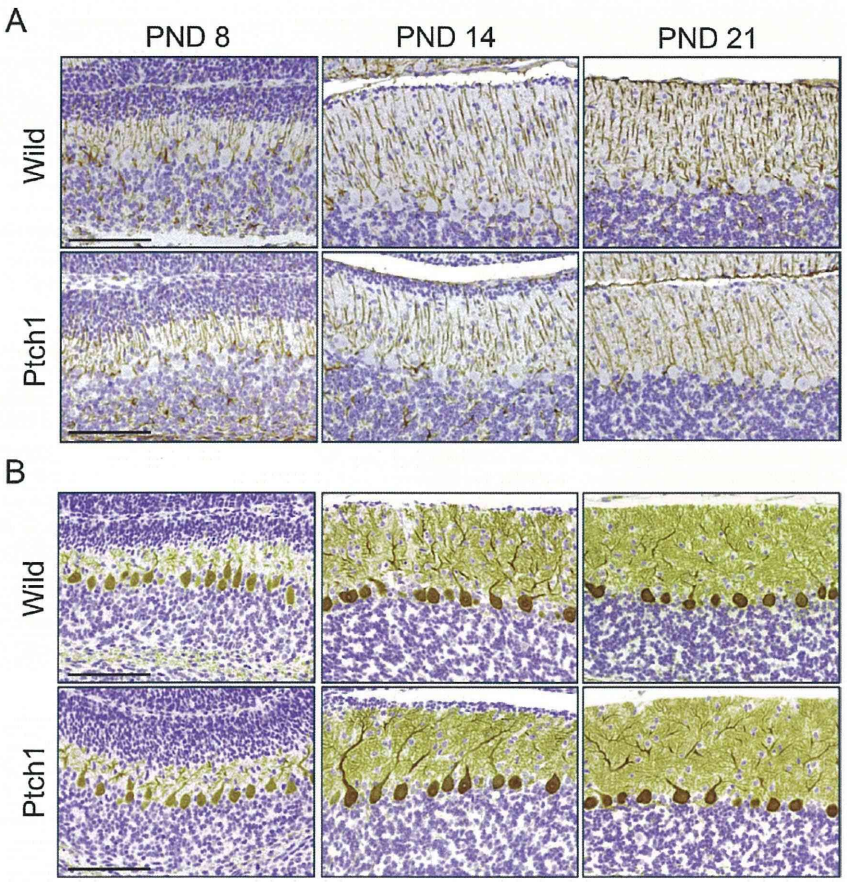

Fig. 4. Bergmann glia and Purkinje cells in the developing cerebellum of wild-type and Ptch1 mice. (A) Bergmann glia of wild-type (top row) and Ptch1 mice (bottom row) stained with anti-GFAP antibody at PND8, 14, and 21. No morphological abnormalities were observed in Ptch1 mice compared to wild-type mice. (B) Purkinje cells of wild-type (top row) and Ptch1 mice (bottom row) stained with anti-Calbindin-D-28K antibody at PND8, 14, and 21. No morphological abnormalities were observed in Ptch1 mice compared to wild-type mice. Scale bars: 100 μm.

anti-Calbindin-D-28K (Sigma–Aldrich, MO, USA) as a Purkinje cell marker. A labeled streptavidin-biotin method was applied for anti-BrdU and Ki-67 antibodies using polyclonal rabbit anti-rat biotinylated IgG (Dako Cytomation) and streptavidin-conjugated horseradish peroxidase (Dako Cytomation). A polymer method was applied for the rest of the primary antibodies using Histofine Simple Stain kit (Nichirei Biosciences Inc., Tokyo, Japan). The immunoreactions were visualized by peroxidase-diaminobenzidine reaction. The sections were then counterstained lightly with hematoxylin. Table 1 provides details of protocols for the immunohistochemistry and information of the antibodies.

2.8. Statistical analysis

The width of the EGL was analyzed by Student's *t*-test following a test for equal variance. The value of one litter per dam or average value of some litters from the same dam was statistically analyzed at PND0, 1, 2, 3, 7, 8, 12 and 14.

3. Results

3.1. General remarks

There were no significant differences in body weight from PND0 to PND21 among the genotypes of intact animals (data not shown). Mortality and body weight of mice were not affected by injection of BrdU. No clinical signs were detected in wild-type and Ptch1 mice. At necropsy, swelling of cerebellum and obscurity of lobular structure with a lack of cerebellar foliation which were diagnosed as MB microscopically were observed in Ptch1 mice at PND28 and W5. Hydrocephalus showing slight dilatation of ventricles of cerebrum and masses of skeletal muscles near the ribs or sternums

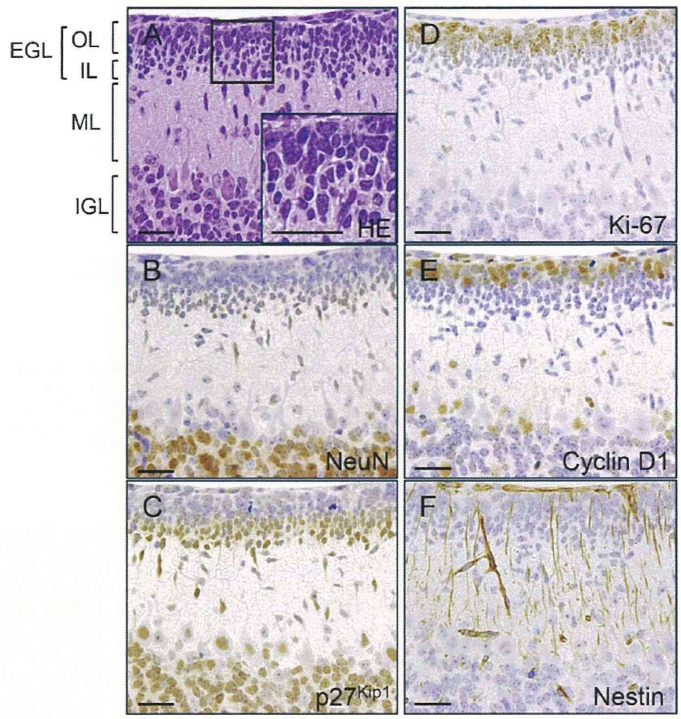

Fig. 5. Morphology and immunohistochemistry of the developing cerebellum. Representative morphology and immunohistochemistry of the developing cerebellar cortex from Ptch1 mice (PND10). Their characteristics were common to both genotypes. (A) HE staining of the cerebellar cortex. EGL framed rectangle was magnified (insert). (B) NeuN was weakly positive in the inner layer of the EGL (IL) and migrating granular cells in the molecular layer (ML) and strongly positive in the IGL. (C) $p27^{kip1}$ was strongly positive in the IL and migrating granular cells in the ML and positive in the IGL. (D) Granular cells in the outer layer of the EGL (OL) were positive for Ki-67. (E) Granular cells in the OL were positive for Cyclin D1. (F) Positive staining for Nestin was observed radically from the surface of the cerebellum to the IGL in a straight line. Scale bars: 25 μm.

and in the abdominal muscles were noted after PND3 in Ptch1 mice only. These intramuscular masses were diagnosed microscopically as rhabdomyosarcomas. Macroscopically, there was no metastatic lesion of MB and rhabdomyosarbomas in tumor-bearing mice.

3.2. Sequential changes in the width and migration process of the EGL

Postnatal changes in the width of the EGL in wild-type and Ptch1 mice are shown in Fig. 2. The width of the EGL peaked at PND4 to 6 and the width in Ptch1 mice was greater than in wild-type mice during first week after birth.

Fig. 3 shows localization of BrdU-positive cells injected in mice at PND8 (Fig. 3A) and PND14 (Fig. 3B), respectively. GCPs in the outer layer of the EGL were the only cell type to be positive for BrdU in the EGL. In animals injected with BrdU at PND8, BrdU-positive cells were observed in the outer layer of the EGL which was positive for Ki-67 1.5 h after the injection (Fig. 3A and 3A inserts). BrdU-positive EGL cells gradually migrated into the IGL accompanied by thinning of the EGL in both genotypes. At PND16, only one layer of the EGL was present and then disappeared at PND21 in both genotypes.

3.3. Sequential changes of Purkinje cells and Bergmann glia in the developing cerebellum

Purkinje cells and Bergmann glia are major components of the cerebellum and have important roles in cerebellar development. Long processes of the radial glial cells, Bergmann glia, were visualized by immunohistochemistry with anti-GFAP antibody (Fig. 4A). For both genotypes, there was no difference in the density or extending direction of the processes at PND0 to 21. In addition, Purkinje neurons (including dendritic arbors) were stained with anti-Calbindin-D-28K antibody (Fig. 4B). From qualitative microscopic inspection a difference in the number, alignment, or arborization of Purkinje cells was not detected between the genotypes during postnatal cerebellar development.

3.4. Morphology and immunohistochemical characteristics of granule cells in the developing cerebellum

Morphology and immunohistochemical reactions to antibodies related to cell proliferation and neuronal differentiation revealed that the structure of the developing cerebellum was common to both genotypes (Table 2 and Fig. 5). Nuclei of GCPs in the outer layer of the EGL were medium to large-sized and round to polygonal. These cells were positive for Ki-67 and Cyclin D1 and negative for

Table 2
Morphological characteristics of granular precursor cells located in EGL, molecular layer, and IGL in developing cerebellum at PND0 to 14.

	EGL		Molecular layer	IGL
	Outer layer	Inner layer		
Histopathology				
	Medium–large size Round–polygonal	Small size Oval–elongate (vertical)	Small size Oval–spindle (vertical)	Medium size Round
Immunohistochemistry				
Ki-67	+	–	–	–
CyclinD1	+	–	–	–
NeuN	–	±	±	+/++
$p27^{kip1}$	–	++	+/++	+
Nestin	+	+	+	±[a]/–[b]

–, negative; ±, weakly positive; +, positive; ++, strongly positive. These characteristics shown in the table are common to all time points measured (PND0 to 14); except for Nestin staining in the IGL.
[a] Until PND10.
[b] Day after PND10.

NeuN and $p27^{kip1}$. Inner layer EGL nuclei were small-sized, oval to elongate, and arranged vertically. In this layer, granular cells were negative for Ki-67 and Cyclin D1, weakly positive for NeuN and strongly positive for $p27^{kip1}$. Migrating granular cells in the molecular layer were oval to spindle shaped small cells arranged vertically and had the same staining profiles as inner layer EGL nuclei. Granular cells with medium-sized round nuclei in the IGL surrounded eosinophilic mossy fibers. Those were negative for Ki-67 and Cyclin D1 and positive to strongly positive for NeuN and $p27^{kip1}$. Positive staining for nestin was observed radically throughout the

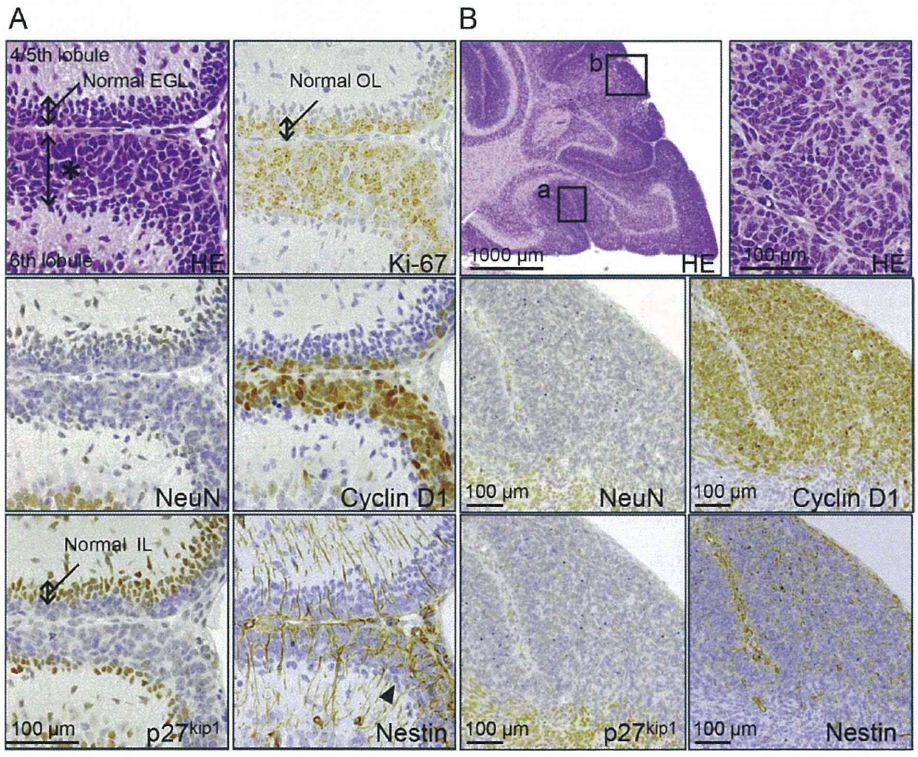

Fig. 6. Proliferative lesions in the developing cerebellum in Ptch1 mice at PND10 and 12. (A) A thickened proliferative lesion (asterisk) in the outer layer of the EGL (6th lobule) in Ptch1 mice at PND10. The 4th/5th lobule showed normal EGL structure. In this lesion, the outer layer of the EGL stained with Ki-67 and cyclinD1 was expanded. The inner layer of the EGL (IL) stained with NeuN and $p27^{kip1}$ was thinned compared to the normal IL in the 4th/5th lobule. Positive staining for Nestin was observed intracellularly in all directions in this lesion (arrowhead). Scale bar: 100 μm. (B) MB in Ptch1 mice at PND12. Higher magnification of rectangle a HE staining showed that proliferating cells resembled thickened lesions of the outer layer of the EGL. The rectangle b showed corresponding area for the pictures stained with NeuN, CyclinD1, $p27^{kip1}$ and Nestin.

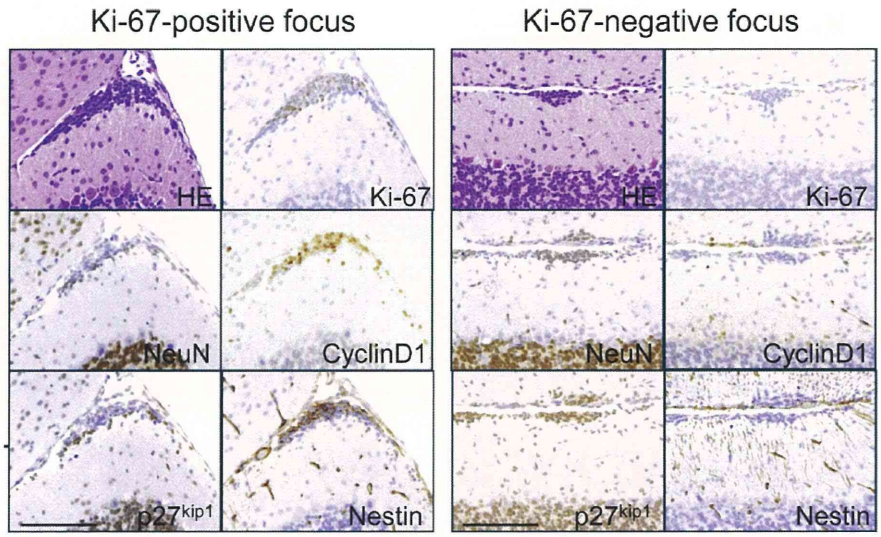

Fig. 7. Immunohistochemical characterization of foci composed of GCP-like cells. Ki-67-positive (left) and Ki-67-negative (right) foci of Ptch1 mice. Ki-67-positive foci were composed of medium to large-sized, round to polygonal nuclei that were negative or weakly positive for NeuN and $p27^{kip1}$ and positive for cyclin D1 and nestin, indicating unclear differentiation into neuronal cells. Ki-67-negative foci were composed of round and small nuclei that were positive for NeuN and $p27^{kip1}$ and negative for Cyclin D1 and nestin, indicating differentiation into neural cells similar to IGL cells. Scale bar: 50 μm.

cerebellar cortex, and weak staining in the IGL remained until PND10.

3.5. Changes in the developing cerebellum and derived cells

Proliferative lesions were observed in the developing cerebellum in Ptch1 mice. Proliferation of GCP-like cells was observed in a thickened area of the EGL, which was continuous from the normal EGL on and after PND10 in Ptch1 mice (Fig. 6A, asterisk). The proliferative lesions substituted for the inner layer of the EGL (Fig. 6A). Moreover, early occurrence of MB was detected at PND12 (Fig. 6B). In both proliferative lesions, large-sized, round to polygonal cells with atypia were main components. Immunohistochemically, the cells were positive for Cyclin D1 and nestin and weakly positive or negative for NeuN and $p27^{kip1}$. Intercellular irregular nestin staining was distinctive of these lesions (Fig. 6A arrowhead and B), as nestin-positive fibers were arranged regularly and radically in a straight line in the normal EGL (Figs. 5F and 6A). Histopathology and immunohistochemistry of these proliferative lesions resembled GCPs in the outer layer of the EGL of the normal cerebellum.

After PND16, the time when migration of EGL cells to the IGL has almost completed, foci with GCP-like cells were detected in the outermost region of the cerebellar cortex in the cerebella of mice from both genotypes (Figs. 3B and 7). In the mice injected with BrdU at PND14, BrdU-positive cells were detected in the EGL 1.5 h after treatment (Fig. 3B) and BrdU-positive cells had migrated into the deep molecular layer and the IGL by PND21 (Fig. 3). As some of the GCP-like cells of the foci in mice injected with BrdU at PND14 were positive for BrdU after PND16, the cells were considered to be derived from the residual GCPs in the EGL (Fig. 3B, arrowhead). The residual foci were clearly classified into two types: Ki-67-positive and Ki-67-negative (Fig. 7). Ki-67-positive foci were composed of atypical cells whose nuclei were medium to large-sized and round to polygonal in shape (Fig. 7, left). The cells were immunohistochemically negative or weakly positive for NeuN and $p27^{kip1}$ and positive for cyclin D1 and nestin (Fig. 7, left). Conversely, Ki-67-negative foci were composed of cells with round and small shaped nuclei. The cells were positive for NeuN and $p27^{kip1}$ and negative for nestin and cyclin D1, indicating differentiation into neural cells (Fig. 7, right). Some of Ki-67-negative foci contained a strongly eosinophilic area resembling mossy fibers among the nuclei (Fig. 8, asterisk) and they were comparable to the structure of the IGL.

3.6. Relationship between residual foci of GCPs and MBs

The incidences of Ki-67-positive or negative foci and MBs were investigated from PND16 up to 10 weeks of age in both genotypes (Fig. 9). MBs were divided into two types: a focal MB occupying one to two lobules of the cerebellum was defined as a small MB and an advanced MB spreading over three or more lobules was defined as a large MB. In Ptch1 mice, Ki-67-positive foci, small MB, and large MB were observed and most of the mice had Ki-67-negative foci. The peak of Ki-67-positive foci was up to PND21, the completion period of cerebellar development. The incidences of MBs were comparable between ages. In wild-type mice, no proliferative lesions, neither Ki-67-positive foci nor MBs other than Ki-67-negative foci, were detected at any age (Fig. 9). The incidence of Ki-67-negative foci decreased with increased age in wild-type mice. The number of Ki-67-negative foci per animal was larger in Ptch1 mice as compared to wild-type mice (data not shown).

Examination for localization of each change revealed that more than 70% of Ki-67-negative foci were localized in the 6–10th lobules of the cerebellum in both genotypes (Fig. 10). In addition, more than 50% of Ki-67-positive foci and small MBs were also observed in the 6–10th lobules in Ptch1 mice (Fig. 10).